Hindawi Publishing Corporation
Journal of Nanomaterials
Volume 2015, Article ID 653192, 9 pages
http://dx.doi.org/10.1155/2015/653192

Research Article

Influence of *In Situ* Oxide Dissolution on the Bottom Morphologies of Detached TiO_2 Nanotube Films

Jia Lin,[1,2] Xiaolin Liu,[2] Shu Zhu,[2] Yongsheng Liu,[1] and Xianfeng Chen[2]

[1]*Department of Physics, Shanghai University of Electric Power, 2103 Pingliang Road, Shanghai 200090, China*
[2]*Department of Physics and Astronomy, Shanghai Jiao Tong University, 800 Dongchuan Road, Shanghai 200240, China*

Correspondence should be addressed to Xianfeng Chen; xfchen@sjtu.edu.cn

Received 20 November 2014; Revised 13 January 2015; Accepted 13 January 2015

Academic Editor: Nageh K. Allam

Free-standing TiO_2 nanotube (NT) films with through holes (i.e., open bottoms) are useful for various applications. In this paper, we report the significant influence of *in situ* chemical etching during the detachment process on the morphological variation of TiO_2 NT bottoms. Under a high temperature detachment anodization, we noted a high detachment rate with controllable bottom morphologies. Influenced by anodization durations, the bottom opening size could be controlled with morphology transition changing from closed to partially open and then to fully open bottoms. The underlying formation mechanism of variable bottom conditions has been examined through the consideration of field-assisted chemical dissolution of both the barrier layer and the sides of the tubes at the bottom. The production of well-defined through-hole tube membranes in a reliable and controllable way is essential for their practical applications.

1. Introduction

The synthesis of self-assembled and well-oriented TiO_2 nanotube (NT) structures by electrochemical anodization has attained much recent attention [1]. Broad and important applications such as sensitized solar cells [2, 3], photo- or photoelectrocatalysis [4, 5], and Li-ion batteries [6] have been proposed. However, TiO_2 NT films grown on opaque Ti metal substrates have certain drawbacks. For example, in dye-sensitized solar cells (DSSCs), the front-side configuration that requires a transparent substrate reaches much higher efficiency than the back-side orientation [7–11]. As a solution, the free-standing membranes have been fabricated and show the following advantages: (a) in the absence of a blocking layer between the NTs and the substrate, the tube membranes can be well connected to conductive substrates, improving the electron transfer performance [12]; (b) previous studies indicate that during crystallization the rutile phase grows at the NT-metal interfaces; this hinders electron transport to the substrate. For membranes without the substrate effect, excellent crystallization can be achieved with pure anatase phase [13]; (c) precrystallized membranes are suitable for low-temperature synthesis of DSSCs on flexible substrates [14, 15]. Self-detachment anodization is a simple but reliable way to produce high quality NTs with controllable thicknesses. However, the resulting membranes generally have closed bottom morphologies, which would deteriorate their performance in various applications.

NTs with a sealed end can trap air inside the tubes making the inner surface of the NTs less accessible [16]. In contrast, through-hole NT structures with open bottoms have more penetration pathways [17]. For example, the open bottom structure in DSSCs has a larger dye adsorption amount and easier transfer of redox ions [18, 19]. Others reported that without the bottom caps the reflection of incident light can be reduced to facilitate electron transport [20]. In quantum dot (QD) sensitized solar cells, through-hole NTs allow the uniform decoration of both inner and outer NT walls with semiconductor QDs [21]. Due to the full access to TiO_2, a through-hole membrane would be desirable for the conversion of CO_2 and water vapor to hydrocarbon fuels because of the flow-through reaction configuration [22, 23]. Tube filling with nanoparticles [24, 25] or nanorods [26, 27] requires the efficient flow of solution into interior of NTs. Other newly

exploited applications of TiO_2 NT membranes, for example, bioactive filters [28, 29], ion exchange membranes [30], and through-hole photocatalysis [31, 32], also require the use of membranes with open tube bottoms by fixing them to supporting frames.

The fabrication of TiO_2 through-hole membranes is an important research topic. The main target is the elimination of the barrier layer that covers the tube bottoms. After the detachment of the membranes, an additional etching procedure by contact with acid etchants solution or vapor can open the closed bottoms [9, 31, 33–36]. During the complex and repeated etching process, membranes may be broken, especially for thin films. A quick method to open the closed bottoms has been developed with the assistance of the reduced or elevated anodization voltages at the end of the anodization process [37–39]. However, the inner diameter of the opened pore is small and the membrane bottom has remnants—this requires an additional etching step to fully open the bottoms [29]. Another direct detachment of tube films at high voltages has no approach to control the objective film morphologies including tube diameter or film thickness [40].

The effectiveness of the through-hole membranes in various applications strongly depends on the specific bottom feature. However, the detailed controlling of bottom morphologies is still a challenge. In the present investigation, transitions of bottom morphologies are distinguished by varying the anodization duration. Furthermore, through the consideration of the TiO_2 dissolution processes, the underlying formation mechanism of various bottom conditions has been discussed. The results show the advantages of this fabrication strategy including the simplicity of the *in situ* fabrication process and uniform membranes with well-controlled bottom opening sizes.

2. Materials and Method

Ti foils (1 cm × 3 cm, thickness 0.89 mm, and 99.7% purity, Alfa Aesar) were cleaned with deionized (DI) water, acetone, and isopropanol successively before anodization. The anodization was performed in a two-electrode arrangement with Ti foil as the working electrode and Pt foil as the counter electrode. The distance between the two electrodes was 3 cm. The electrolyte solution was composed of 0.5 wt% NH_4F and 3 vol% DI water in ethylene glycol. TiO_2 NT array films were prepared by three-step anodization at a constant voltage of 60 V. Firstly, Ti foil was preanodized at a bath temperature of 20°C for 1 h. The oxide film grown at the Ti surface was then removed by ultrasonication to achieve defined patterns for further tube growth. The second-step anodization was then adopted to grow well-aligned and highly ordered TiO_2 NT arrays in the same electrolyte at 20°C. The resulting NT films (first step 1 h + second step 1 h) were subjected to thermal treatment (200°C) in air for 1 h [41]. For comparison, the films were also annealed at a higher temperature of 300°C. The NT layers were next subjected to a successive third-step anodization process in the same electrolyte but with an elevated bath temperature of 30°C. The anodization duration was adjusted in the range of 0.5–2 h to investigate variations in bottom morphology. The third anodization eventually caused the detachment of the tube layer from the Ti foil. After the anodization processes, the detached free-standing NT films were cleaned with ethanol and dried in air repeatedly. The anodic current densities were recorded by a SourceMeter (Keithley 2400). The morphologies were analyzed with a field-emission scanning electron microscope (FE-SEM, FEI Sirion 200). The crystal structures were measured by X-ray diffraction (XRD, Cu K_α radiation, Rigaku 9KW SmartLab) patterns.

3. Results and Discussion

In a general electrochemical growth process, the dissolution process plays an important role in the structural and morphological variations of TiO_2 NTs. This is influenced by the anodic environment such as voltage, water, and fluoride ion (F^-) concentration, duration, electrolyte viscosity, and bath temperature. According to the mechanistic model of NT formation by anodization, two main reactions exist at the anode—the formation of the oxide layer and the dissolution process [42]. Basically, the continuous dissolution of oxide and oxidation of metal at the electrolyte/oxide and oxide/metal interfaces determine the complex kinetic process of tube growth [43–45].

The effect of dissolution can be seen in the significant variation of the average NT inner diameter at the top of the layer during the first two anodization steps. As the anodization reaction proceeded, the tube wall became thinner and the tube inner diameter increased (the variation of the bottom morphology is similar and is discussed below). By increasing the duration from 0.5 to 2 h, the average inner diameter increased from ~80 to 127 nm as estimated by top-view SEM images. However, the outer diameter changed much more slowly than the inner diameter. This suggests that the surface dissolution of tubes by the fluoride in the organic electrolyte during anodization is significant.

Unlike tops with open pores, a barrier layer typically covers the tube bottom and thus is closed. The third-step anodization under a high reaction temperature offered a high growth rate and also a high dissolution rate. This detached the NT films and also opened the closed bottom ends [41]. We found that the current densities increased with a rise in bath temperature. Figure 1 shows the anodic current densities recorded during the second and third steps. Both of the two curves showed a sharp current rise in the initial stage, but the current recovery of the third step was much slower due to the electrolyte penetration through the top NT film before NT growth underneath. For NT growth at the second step, the current density showed a decreasing tendency with anodization time during the oxidation process. However, the current profile was quite uniform at the third step. The gradual detachment of the NT film from the underlying Ti substrate resulted in the increase of current density since the top NT layer would not impede the new NT growth any longer.

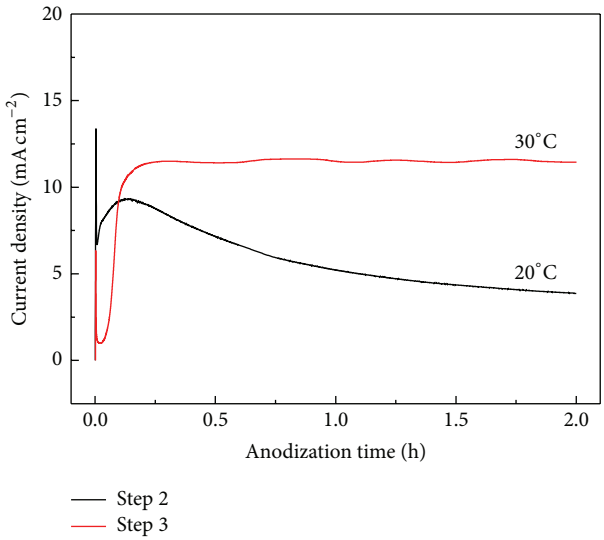

FIGURE 1: The variations of anodic current densities with time during the second and the third steps.

During conventional anodic tube fabrication, the dissolution of oxides is attributed to the etching by F^-, which can also be promoted by the presence of H^+. The rapid third-step anodization generated more H^+ at the bottom and led to decreased pH. Thus oxide dissolution at the tube bottom was comparatively high, resulting in film detachment and bottom opening (Figures 2(a)–2(c)). Figure 2(d) shows the optical image of the detached through-hole film (~1 cm × 1 cm). From XRD patterns shown in Figure 3, it is obvious that no anatase (101) main peak was observed when the films were annealed at 200°C between the second and third steps. The TiO_2 films maintained their amorphous character, showing the dark color. This facilitated the dissolution of the NT bottom during the detachment anodization. However, for NT films annealed at an elevated temperature of 300°C or above, the NT films were crystallized to anatase phase (Figure 3). Due to the high stability of anatase NTs, tube membranes with closed bottoms were obtained.

The relationship between membrane bottom morphology and experimental parameters is now discussed. Figure 4 demonstrates the variation of back-side morphologies as a function of detachment time. The NTs showed a double-layered structure before detachment with an interface. From the cross-sectional images, the duration affected the bottom morphology of TiO_2 NTs. From Figures 4(a) and 4(b), the bottom caps gradually disappeared along with the formation of open bottoms at some regions. Figure 4(c) shows that after a lengthy etching the barrier layer was totally dissolved and thus the entire bottom was open. This suggests that dissolution time of the tube bottom is a key parameter governing the opening of the bottoms.

To investigate the possible mechanism of bottom opening, the detailed bottom structure was examined. Figure 5(a) shows that the barrier layer connected to the bottom was not dense, which facilitated the penetration of ions through the barrier oxide layer at the tube bottom with the assistance of an electric field across the layer. Figure 5(b) shows that in some regions at the bottom the detachment of the bottom barrier layer as a whole emerged after the crystallization of the NTs with closed bottoms. This suggests that the tube bottom is loosely connected to the upper region and thus can be separated.

Near the bottom positions, the tube walls consisted of two shells with a double-walled NT morphology (Figure 5(c)). As has been reported, the Ti cation (Ti^{4+}) upwards to the oxide/electrolyte interface and oxygen anion (O^{2-}) downwards to the oxide/metal interface under anodic field across the bottom oxide can form new oxides at both interfaces [46]. However, because the upper oxide/electrolyte interface was more accessible to F^- or carbon ions in the electrolyte [47], the resulting oxide tube walls were separated into two shells. During the anodization formation process, the dissolution of the two sides (inner and outer) of the tubes was different. The inner shell was in direct contact with the electrolyte and was unstable and prone to dissolution. As a result, when the anodization was prolonged, the inner shell gradually dissolved and the inner diameter increased. This is consistent with a great increase in tube inner diameter for longer anodization times as discussed above. Due to the double-shell nature of the tube wall, a special morphology would form at the bottom after film detachment. At the bottom, tube sidewalls showed two shells with evident interfaces (discussed below).

Based on the above studies, we suggested a plausible explanation of the chemical etching process at the bottom subjected to the F^--containing electrolyte. During the detachment, the bottom interface dissolved due to the F^- rich region existing underneath the tubes and over the outer tube surfaces (Figure 6(a)). The F^- rich layer originated from the accumulation of F^- at the metal/oxide interface during tube growth. This can be explained by a flow model [48, 49]. The dissolution of this layer led to the detachment of the films and the separation of tubes at cell boundaries. As discussed in Figure 2, the anodization formed a new layer of oxide tubes accompanied by the generation of hydrogen ions leading to aggressive acid attack near the bottom region (Figure 6(b)).

Importantly, the high detachment temperature increased the ion diffusivity [50]. To realize new tube growth under the NT films, anions (O^{2-} and F^-) should migrate downwards through the bottom cap via the high electric field to arrive at the base of the underlying tubes (Figure 6(a)). The current densities through the barrier layer were very high at high temperatures, which implied a superior migration rate of F^- from the bulk electrolyte towards the reaction region. As a result, the bottom of the tubes was gradually perforated due to significant chemical dissolution during the ionic transport. Afterwards, the small pores at the tube bottom were enlarged due to the etching of the unstable inner shell of the tubes—this altered the bottom morphology from being closed to open.

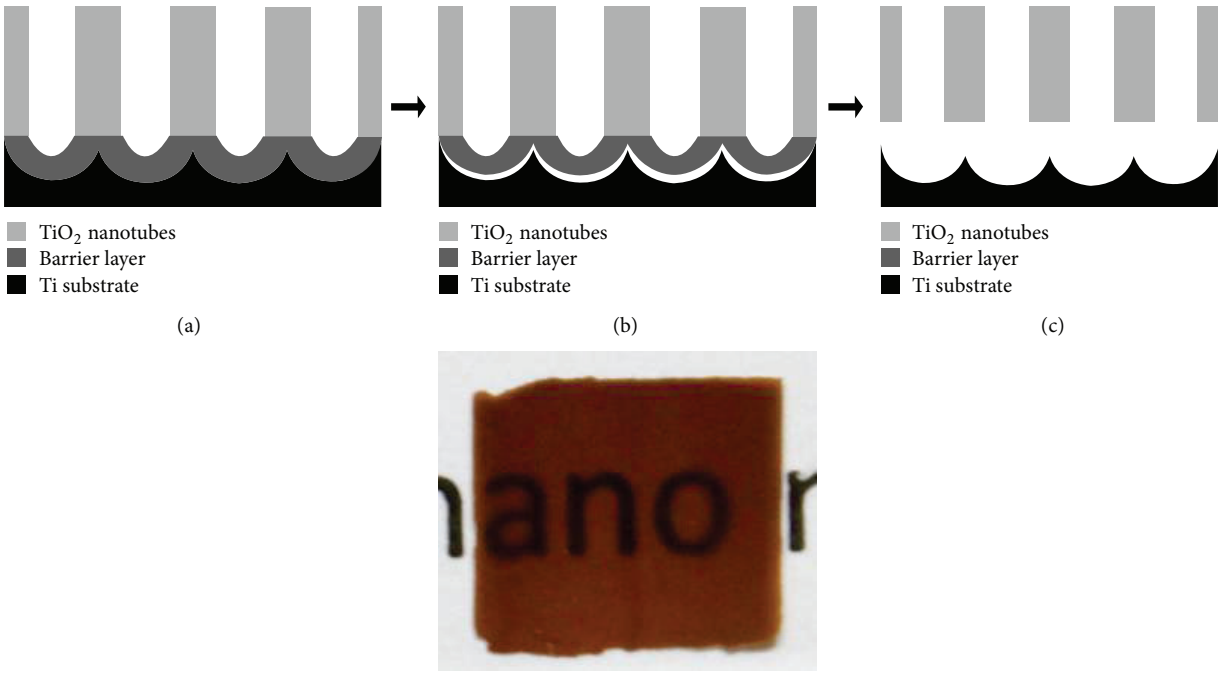

Figure 2: ((a)–(c)) The fabrication procedure of free-standing and through-hole NT films and (d) the image of through-hole film.

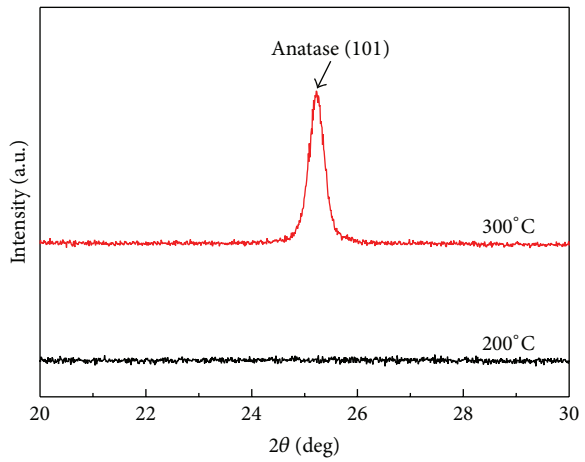

Figure 3: XRD patterns of NT membranes annealed at 200 and 300°C before detachment.

Furthermore, in the bottom side, as the anodization proceeds rapidly, heat was continuously generated during the growth. As the diffusion process was relatively slow, a large amount of heat evolved locally near the bottom of the tubes and established the temperature gradient along the tube. The great change in local temperature under the oxide film possibly accelerated the dissolution of the barrier layer. Considering the high-field model to be the main mechanism [51], we plotted the relationship between $f(i) = \sqrt{-di/dt}/i$ and $\ln i$ at two temperatures via statistical analysis of the current data (Figure 7). The relationship between $f(i)$ and $\ln i$ was not perfectly linear. The slope, which was proportional to the square root of the absolute temperatures $\sqrt{T}$, increased with time. That is, $\ln i$ became smaller as the anodization proceeded implying that the increase in local temperature was due to the reaction heat. New tube growth below the previously formed tube bottom led to preferential chemical etching at the bottom cap, and thus the barrier layer became thinner.

The bottom morphology evolution as a result of *in situ* etching during the film separation from the Ti foil is shown in Figure 8. As the detachment anodization proceeded, the bottom barrier oxide layer was gradually thinned and the tube bottom partially opened. Notably, some portion of the tube bottom was covered by remnants (white part in Figure 8(a)) if the duration was not sufficiently long. This resulted in relatively rough bottoms. The remnants were actually the interface F^- rich layer between the oxide NT array and the underlying Ti metal substrate and/or the top of the newly formed oxide layer. The intertube region was also filled with a F^- rich layer. Afterwards, extended anodization completely consumed the barrier layer and consequently the bottoms were fully open (Figure 8(b)). The tube walls showed double shells with inner/outer shell boundaries. The inner diameter of the tubes near the bottom was much smaller than those at the top due to the thick inner shell at the bottom. Further increased duration of dissolution led to thinning of the inner shell of the sidewalls, and the narrow tube mouth was enlarged. Also, the shape of the open ends changed from being hexagonally arranged to round at the bottom

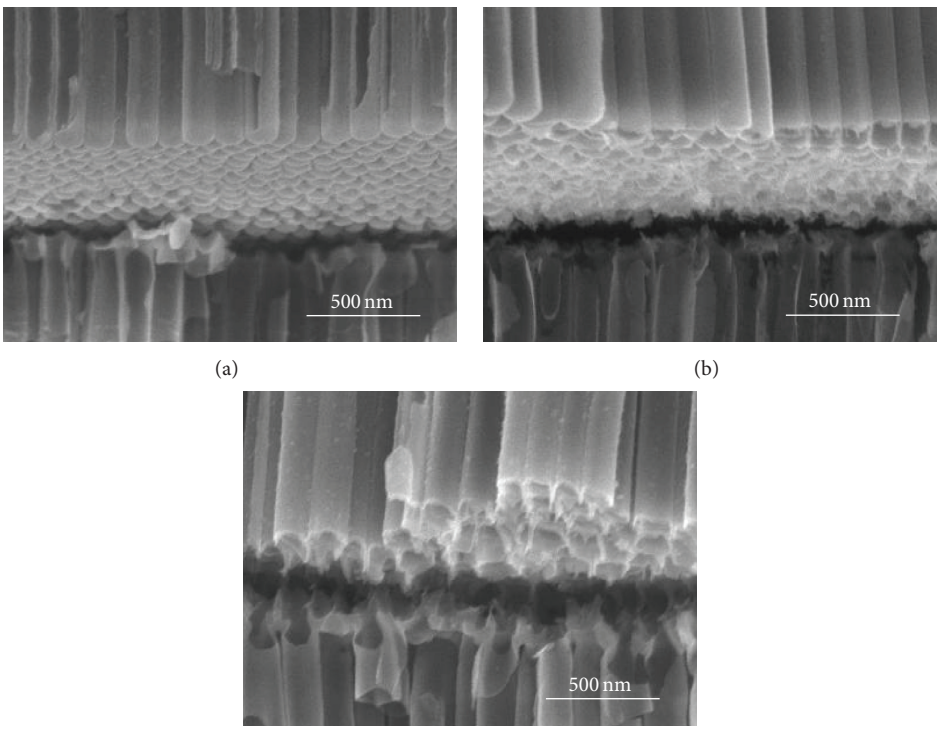

(a) (b)

(c)

Figure 4: Cross-sectional SEM of the dissolved interface between the tube bottom and the newly formed tubes. The bottom morphology of the upside layer changed from (a) closed to (b) partially open and finally to (c) fully open bottom ends. This corresponds to the third-step anodization time of (a) 15 min, (b) 30 min, and (c) 60 min.

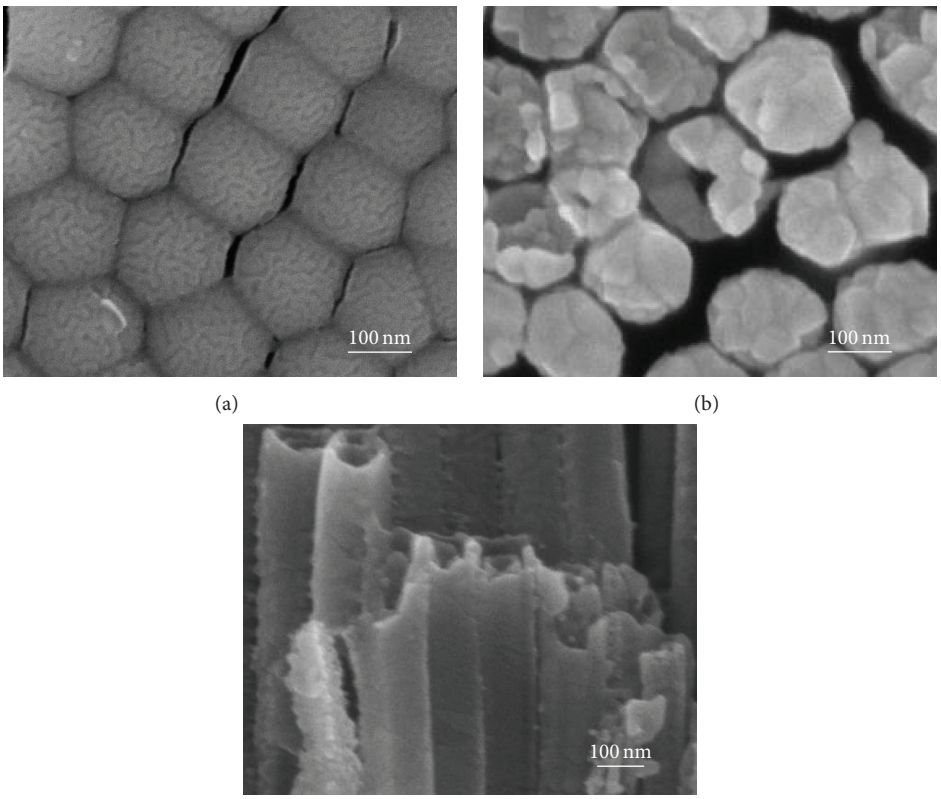

(a) (b)

(c)

Figure 5: High magnification SEM images of tube bottoms and sides: (a) the loose bottoms, (b) annealed bottoms showing the barrier layer, and (c) the side view of tubes near the bottom showing two shells of tube walls.

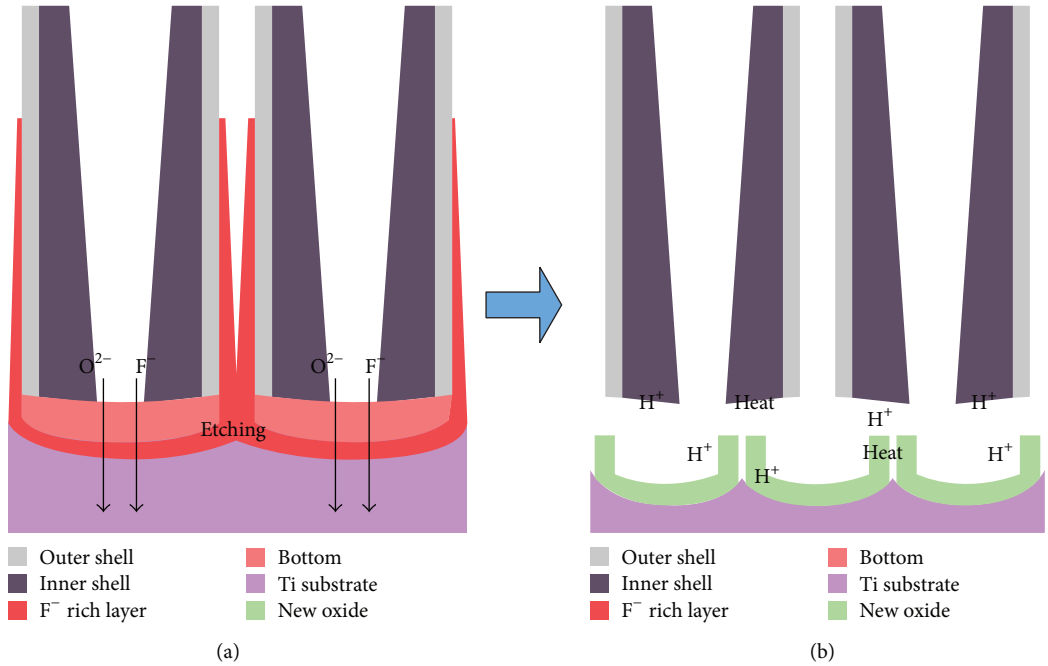

Figure 6: Schematic of the opening of the back side of free-standing layers.

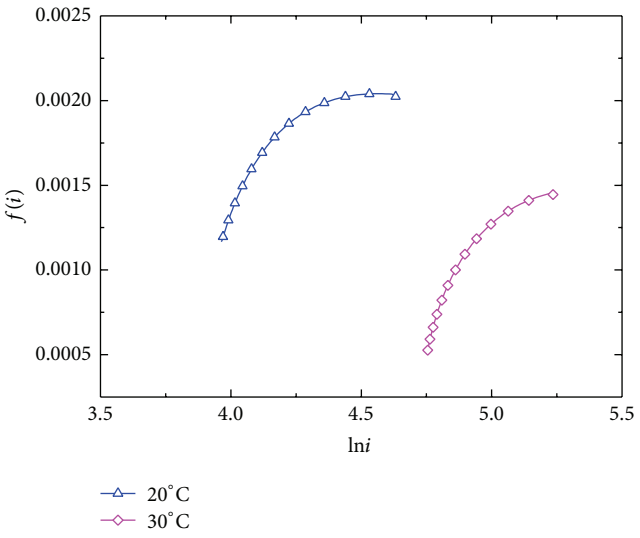

Figure 7: The $f(i)$-ln$i$ relation based on the analysis of the current-time curve.

(Figure 8(c)). After prolonged anodization, the tube inner wall was completely dissolved. This resulted in membranes with highly opened tubes. The SEM image of high quality and uniform open tubes on the bottom side is shown in Figure 8(d).

From the above discussion, detachment and bottom opening occurred simultaneously in *in situ* etching and the opening of pore bottoms was obtained. An increase in bottom opening size (from ~60.3 to 123.5 nm) came from extended anodization. This is similar to the variation in the surface diameter. That is to say, the size of the bottom opening is dependent on the degree of dissolution. However, the outer walls changed slightly during the film detachment, which was evident from similar intertube spacing values. It should be noted that during the detachment the NT films remained partially connected to the substrate. The smooth tube bottoms with a large diameter may lead to more accessible inner surfaces of NTs to improve their performance.

4. Conclusions

In the above work, geometric modification of NT bottom morphologies was greatly affected by anodization temperature and duration. The detachment of tube membranes and the opening of tube bottoms were achieved by *in situ* chemical etching during anodization. Various open bottom structures could conceivably be obtained as a consequence of the influence of dissolution of the bottom interface layer, barrier layer, and tube sidewalls. The degree of pore enlargement at the bottom increased as the anodization time increased, resulting in the easy adjustment of bottom opening of the membrane layer. These results indicate a useful route to improve the NT morphology and inspire further applications of through-hole TiO_2 NTs.

Conflict of Interests

The authors declare that there is no conflict of interests regarding the publication of this paper.

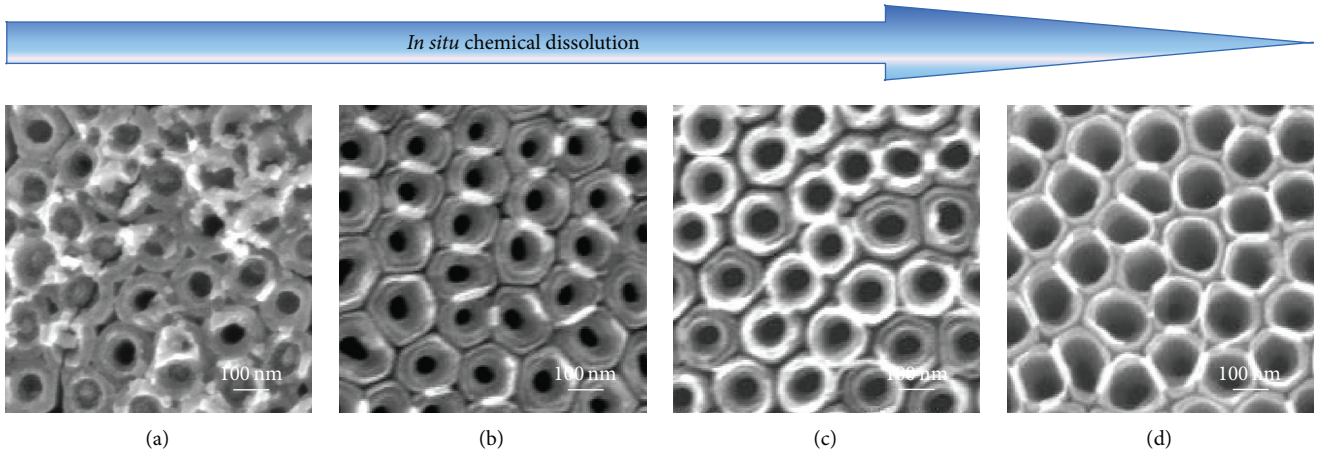

FIGURE 8: The transitions of back-side morphology. (a) Partially open bottoms. Fully open bottoms with (b) small, (c) middle, and (d) large bottom openings corresponding to detachment anodization times of 0.5, 1, 1.5, and 2 h, respectively.

Acknowledgments

The work was supported by the National Natural Science Foundation of China (Grant nos. 61125503 and 61404081) and the Shanghai Municipal Natural Science Foundation (Grant no. 14ZR1417700).

References

[1] M. Paulose, K. Shankar, S. Yoriya et al., "Anodic growth of highly ordered TiO_2 nanotube arrays to 134 μm in length," *The Journal of Physical Chemistry B*, vol. 110, no. 33, pp. 16179–16184, 2006.

[2] G. K. Mor, O. K. Varghese, M. Paulose, K. Shankar, and C. A. Grimes, "A review on highly ordered, vertically oriented TiO_2 nanotube arrays: fabrication, material properties, and solar energy applications," *Solar Energy Materials and Solar Cells*, vol. 90, no. 14, pp. 2011–2075, 2006.

[3] K. G. Ong, O. K. Varghese, G. K. Mor, K. Shankar, and C. A. Grimes, "Application of finite-difference time domain to dye-sensitized solar cells: the effect of nanotube-array negative electrode dimensions on light absorption," *Solar Energy Materials and Solar Cells*, vol. 91, no. 4, pp. 250–257, 2007.

[4] V. Müller and P. Schmuki, "Efficient photocatalysis on hierarchically structured TiO_2 nanotubes with mesoporous TiO_2 filling," *Electrochemistry Communications*, vol. 42, pp. 21–25, 2014.

[5] J. Liu, Z. Y. Liu, T. R. Zhang, J. Zhai, and L. Jiang, "Low-temperature crystallization of anodized TiO_2 nanotubes at the solid-gas interface and their photoelectrochemical properties," *Nanoscale*, vol. 5, no. 13, pp. 6139–6144, 2013.

[6] Z. G. Lu, C.-T. Yip, L. P. Wang, H. T. Huang, and L. M. Zhou, "Hydrogenated TiO_2 nanotube arrays as high-rate anodes for lithium-ion microbatteries," *ChemPlusChem*, vol. 77, no. 11, pp. 991–1000, 2012.

[7] X. K. Xin, J. Wang, W. Han, M. D. Ye, and Z. Q. Lin, "Dye-sensitized solar cells based on a nanoparticle/nanotube bilayer structure and their equivalent circuit analysis," *Nanoscale*, vol. 4, no. 3, pp. 964–969, 2012.

[8] K. Shankar, G. K. Mor, M. Paulose, O. K. Varghese, and C. A. Grimes, "Effect of device geometry on the performance of TiO_2 nanotube array-organic semiconductor double heterojunction solar cells," *Journal of Non-Crystalline Solids*, vol. 354, no. 19–25, pp. 2767–2771, 2008.

[9] Q. Chen and D. Xu, "Large-scale, noncurling, and free-standing crystallized TiO_2 nanotube arrays for dye-sensitized solar cells," *The Journal of Physical Chemistry C*, vol. 113, no. 15, pp. 6310–6314, 2009.

[10] M. Dubey, M. Shrestha, Y. H. Zhong, D. Galipeau, and H. S. He, "TiO_2 nanotube membranes on transparent conducting glass for high efficiency dye-sensitized solar cells," *Nanotechnology*, vol. 22, no. 28, Article ID 285201, 2011.

[11] L.-L. Li, Y.-J. Chen, H.-P. Wu, N. S. Wang, and E. W.-G. Diau, "Detachment and transfer of ordered TiO_2 nanotube arrays for front-illuminated dye-sensitized solar cells," *Energy and Environmental Science*, vol. 4, no. 9, pp. 3420–3425, 2011.

[12] G. H. Liu, T. Chen, Y. L. Sun, G. Chen, and K. Y. Wang, "Transferable, conductive TiO_2 nanotube membranes for opto-electronics," *Applied Surface Science*, vol. 311, pp. 529–533, 2014.

[13] J. Lin, M. Guo, C. T. Yip et al., "High temperature crystallization of free-standing anatase TiO_2 nanotube membranes for high efficiency dye-sensitized solar cells," *Advanced Functional Materials*, vol. 23, no. 47, pp. 5952–5960, 2013.

[14] Y.-Y. Kuo and C.-H. Chien, "Sinter-free transferring of anodized TiO_2 nanotube-array onto a flexible and transparent sheet for dye-sensitized solar cells," *Electrochimica Acta*, vol. 91, pp. 337–343, 2013.

[15] F. Bella, A. Lamberti, A. Sacco, S. Bianco, A. Chiodoni, and R. Bongiovanni, "Novel electrode and electrolyte membranes: towards flexible dye-sensitized solar cell combining vertically aligned TiO_2 nanotube array and light-cured polymer network," *Journal of Membrane Science*, vol. 470, pp. 125–131, 2014.

[16] D. Kim, J. M. Macak, F. Schimidt-Stein, and P. Schmuki, "Capillary effects, wetting behavior and photo-induced tube filling of TiO_2 nanotube layers," *Nanotechnology*, vol. 19, no. 30, Article ID 305710, 2008.

[17] G. H. Liu, K. Y. Wang, N. Hoivik, and H. Jakobsen, "Progress on free-standing and flow-through TiO_2 nanotube membranes," *Solar Energy Materials and Solar Cells*, vol. 98, pp. 24–38, 2012.

[18] S. Kathirvel, C. Su, C. Hsu, S.-Y. Ho, B.-R. Chen, and W.-R. Li, "Effect of open- and close-ended TiO_2 nanotube arrays on transparent conducting substrates for dye-sensitized solar cells application," *Journal of Nanoparticle Research*, vol. 16, no. 5, article 2377, 2014.

[19] J. Choi, S. Song, G. Kang, and T. Park, "Dye-sensitized solar cells employing doubly or singly open-ended TiO_2 nanotube arrays: structural geometry and charge transport," *ACS Applied Materials & Interfaces*, vol. 6, no. 17, pp. 15388–15394, 2014.

[20] C. Rho, J.-H. Min, and J. S. Suh, "Barrier layer effect on the electron transport of the dye-sensitized solar cells based on TiO_2 nanotube arrays," *The Journal of Physical Chemistry C*, vol. 116, no. 12, pp. 7213–7218, 2012.

[21] S. Gao, J. Y. Yang, M. Liu et al., "Enhanced photovoltaic performance of CdS quantum dots sensitized highly oriented two-end-opened TiO_2 nanotubes array membrane," *Journal of Power Sources*, vol. 250, pp. 174–180, 2014.

[22] O. K. Varghese, M. Paulose, T. J. LaTempa, and C. A. Grimes, "High-rate solar photocatalytic conversion of CO_2 and water vapor to hydrocarbon fuels," *Nano Letters*, vol. 9, no. 2, pp. 731–737, 2009.

[23] S. C. Roy, O. K. Varghese, M. Paulose, and C. A. Grimes, "Toward solar fuels: photocatalytic conversion of carbon dioxide to hydrocarbons," *ACS Nano*, vol. 4, no. 3, pp. 1259–1278, 2010.

[24] J. Choi, Y. S. Kwon, and T. Park, "Doubly open-ended TiO_2 nanotube arrays decorated with a few nm-sized TiO_2 nanoparticles for highly efficient dye-sensitized solar cells," *Journal of Materials Chemistry A*, vol. 2, no. 35, pp. 14380–14385, 2014.

[25] H. D. Bian, Y. Wang, B. Yuan et al., "Flow-through TiO_2 nanotube arrays: a modified support with homogeneous distribution of Ag nanoparticles and their photocatalytic activities," *New Journal of Chemistry*, vol. 37, no. 3, pp. 752–760, 2013.

[26] D. Fang, K. L. Huang, S. Q. Liu, and D. Y. Qin, "High density copper nanowire arrays deposition inside ordered titania pores by electrodeposition," *Electrochemistry Communications*, vol. 11, no. 4, pp. 901–904, 2009.

[27] D. A. Wang and L. F. Liu, "Continuous fabrication of free-standing TiO_2 nanotube array membranes with controllable morphology for depositing interdigitated heterojunctions," *Chemistry of Materials*, vol. 22, no. 24, pp. 6656–6664, 2010.

[28] M. Paulose, L. Peng, K. C. Popat et al., "Fabrication of mechanically robust, large area, polycrystalline nanotubular/porous TiO_2 membranes," *Journal of Membrane Science*, vol. 319, no. 1-2, pp. 199–205, 2008.

[29] J. Schweicher and T. A. Desai, "Facile synthesis of robust free-standing TiO_2 nanotubular membranes for biofiltration applications," *Journal of Applied Electrochemistry*, vol. 44, no. 3, pp. 411–418, 2014.

[30] B. Zhu, J. J. Li, Q. W. Chen, R.-G. Cao, J. M. Li, and D. S. Xu, "Artificial, switchable K^+-gated ion channels based on flow-through titania-nanotube arrays," *Physical Chemistry Chemical Physics*, vol. 12, no. 34, pp. 9989–9992, 2010.

[31] S. P. Albu, A. Ghicov, J. M. Macak, R. Hahn, and P. Schmuki, "Self-organized, free-standing TiO_2 nanotube membrane for flow-through photocatalytic applications," *Nano Letters*, vol. 7, no. 5, pp. 1286–1289, 2007.

[32] J. J. Liao, S. W. Lin, N. Q. Pan, D. H. Li, S. P. Li, and J. B. Li, "Free-standing open-ended TiO_2 nanotube membranes and their promising through-hole applications," *Chemical Engineering Journal*, vol. 211-212, pp. 343–352, 2012.

[33] D. Fang, K. L. Huang, S. Q. Liu, Z. P. Luo, X. X. Qing, and Q. G. Zhang, "High-density $NiTiO_3/TiO_2$ nanotubes synthesized through sol-gel method using well-ordered TiO_2 membranes as template," *Journal of Alloys and Compounds*, vol. 498, no. 1, pp. 37–41, 2010.

[34] C.-J. Lin, W.-Y. Yu, and S.-H. Chien, "Transparent electrodes of ordered opened-end TiO_2-nanotube arrays for highly efficient dye-sensitized solar cells," *Journal of Materials Chemistry*, vol. 20, no. 6, pp. 1073–1077, 2010.

[35] S. Banerjee, M. Misra, S. K. Mohapatra, C. Howard, S. K. Mohapatra, and S. K. Kamilla, "Formation of chelating agent driven anodized TiO_2 nanotubular membrane and its photovoltaic application," *Nanotechnology*, vol. 21, no. 14, Article ID 145201, 2010.

[36] J. Choi, S.-H. Park, Y. S. Kwon, J. Lim, I. Y. Song, and T. Park, "Facile fabrication of aligned doubly open-ended TiO_2 nanotubes, via a selective etching process, for use in front-illuminated dye sensitized solar cells," *Chemical Communications*, vol. 48, no. 70, pp. 8748–8750, 2012.

[37] Y. Jo, I. Jung, I. Lee, J. Choi, and Y. Tak, "Fabrication of through-hole TiO_2 nanotubes by potential shock," *Electrochemistry Communications*, vol. 12, no. 5, pp. 616–619, 2010.

[38] S. Q. Li and G. M. Zhang, "One-step realization of open-ended TiO_2 nanotube arrays by transition of the anodizing voltage," *Journal of the Ceramic Society of Japan*, vol. 118, no. 1376, pp. 291–294, 2010.

[39] Z.-Y. Luo, D.-C. Mo, and S.-S. Lu, "The key factor for fabricating through-hole TiO_2 nanotube arrays: a fluoride-rich layer between Ti substrate and nanotubes," *Journal of Materials Science*, vol. 49, no. 19, pp. 6742–6749, 2014.

[40] H. M. Ouyang, G. T. Fei, Y. Zhang et al., "Large scale free-standing open-ended TiO_2 nanotube arrays: stress-induced self-detachment and in situ pore opening," *Journal of Materials Chemistry C*, vol. 1, no. 45, pp. 7498–7506, 2013.

[41] J. Lin, J. F. Chen, and X. F. Chen, "Facile fabrication of free-standing TiO_2 nanotube membranes with both ends open via self-detaching anodization," *Electrochemistry Communications*, vol. 12, no. 8, pp. 1062–1065, 2010.

[42] A. Ghicov and P. Schmuki, "Self-ordering electrochemistry: a review on growth and functionality of TiO_2 nanotubes and other self-aligned MO_x structures," *Chemical Communications*, no. 20, pp. 2791–2808, 2009.

[43] K. R. Hebert, S. P. Albu, I. Paramasivam, and P. Schmuki, "Morphological instability leading to formation of porous anodic oxide films," *Nature Materials*, vol. 11, no. 2, pp. 162–166, 2012.

[44] S. Huang, W. Peng, C. Ning, Q. Hu, and H. Dong, "Nanostructure transition on anodic titanium: structure control via a competition strategy between electrochemical oxidation and chemical etching," *The Journal of Physical Chemistry C*, vol. 116, no. 1, pp. 22359–22364, 2012.

[45] D. Kowalski, D. Kim, and P. Schmuki, "TiO_2 nanotubes, nanochannels and mesosponge: self-organized formation and applications," *Nano Today*, vol. 8, no. 3, pp. 235–264, 2013.

[46] N. Liu, H. Mirabolghasemi, K. Lee et al., "Anodic TiO_2 nanotubes: double walled *vs.* single walled," *Faraday Discussions*, vol. 164, pp. 107–116, 2013.

[47] S. P. Albu, A. Ghicov, S. Aldabergenova et al., "Formation of double-walled TiO_2 nanotubes and robust anatase membranes," *Advanced Materials*, vol. 20, no. 21, pp. 4135–4139, 2008.

[48] S. Berger, S. P. Albu, F. Schmidt-Stein et al., "The origin for tubular growth of TiO_2 nanotubes: a fluoride rich layer between tube-walls," *Surface Science*, vol. 605, no. 19-20, pp. L57–L60, 2011.

[49] S. J. Garcia-Vergara, P. Skeldon, G. E. Thompson, and H. Habazaki, "A flow model of porous anodic film growth on aluminium," *Electrochimica Acta*, vol. 52, no. 2, pp. 681–687, 2006.

[50] K. Lee, J. Kim, H. Kim et al., "Effect of electrolyte conductivity on the formation of a nanotubular TiO_2 photoanode for a dye-sensitized solar cell," *Journal of the Korean Physical Society*, vol. 54, no. 3, pp. 1027–1031, 2009.

[51] H. E. Prakasam, K. Shankar, M. Paulose, O. K. Varghese, and C. A. Grimes, "A new benchmark for TiO_2 nanotube array growth by anodization," *The Journal of Physical Chemistry C*, vol. 111, no. 20, pp. 7235–7241, 2007.